2013 IEEE/RSJ International Conference on
Intelligent Robots and Systems (IROS)
November 3-7, 2013. Tokyo, Japan

A Modular Actuator with Translational Motion Along an Arc

Arthur E. Quaid[1]

Abstract— **Arctuator modules are modular actuators that provide translational motion along an arc. A motor mounted on one link of a parallelogram four-bar linkage directly drives the opposite link via a cable, gear, or friction drive. Any of the four links can be used as the base or output link, depending on whether relatively high force translational motion, relatively high motion range translational motion, or rotational motion is desired. Appropriately combining multiple modules yields devices that can provide planar or spatial translational motions. Concept designs that combine multiple Arctuator modules depict how the modules can be used for manipulation, fabrication, locomotion, and other applications. Experimental results demonstrate that a prototype Arctuator module is capable of accelerating a cantilevered load of double its own mass upward at 1 g.**

I. Introduction

A common application for robotics is to position an object or tool without changing its orientation. In some cases, Cartesian robots with multiple serial prismatic joints are used. However, prismatic joints present significant design challenges. Unlike revolute joints, which can use compact, precise, low-cost anti-friction rotational bearings, linear guides are larger, heavier, more expensive, and more difficult to maintain. For example, linear guide surfaces must maintain their surface properties and geometry over the entire length of motion. These surfaces are also susceptible to wear, dirt, and moisture, and are difficult to cover and protect[1].

In practice, serial-chain robots with revolute joints are often used for these tasks. However, these revolute joint robots require extra joints to keep the object's orientation from changing. For example, to translate an object in two dimensions without changing its orientation, only two prismatic joints are required. For the same task, three revolute joints are required, increasing the cost and complexity of the device.

For precision positioning of objects over small distances, four-bar linkages with leaf-spring flexures may be used instead. When restricted to motion ranges that are small relative to the lengths of the leaf-spring flexure elements, these devices produce precise near-linear motion. However the joint stiffness of flexures is limited, especially when designed for larger motion ranges[2].

II. Arctuator[2] Modules

An Arctuator module is a parallelogram four-bar linkage with a motor, transmission, and other components packaged within the volume of the linkage, as shown in Fig. 1. The key feature of an Arctuator module is that the motor, mounted on one link, the *drive link*, directly drives the opposite link, the *driven link*. As the motor rotates, the motor pinion rolls along the drive surface, causing the driven link to translate along an arc. The coupling between the motor pinion and drive surface can be a gear, cable, or friction drive depending on the application requirements.

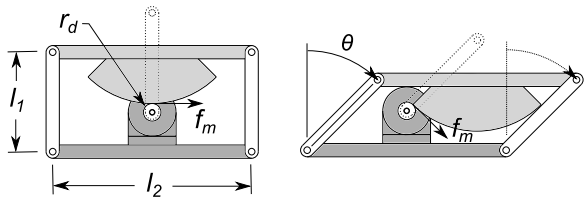

Fig. 1. An Arctuator module includes a motor, transmission, and other components packaged within a four bar parallelogram linkage. A motor on the *drive* link (dark gray) directly applies force f_m to the opposite *driven* link (light gray), causing it to translate along an arc with radius l_1.

Key parameters of the module shown in Fig. 1. Opposite links are of equal length and therefore will remain parallel to one another. Link lengths l_1 and l_2 are design parameters while θ serves as the joint variable for the module. The effective drive radius r_d is important in determining the transmission ratio and the resulting force output capability of the module. A virtual "fifth link" can be imagined between the center of the motor shaft and the center of the drive surface of the driven link. This virtual link will have the same length as the side links (l_1) and stay parallel to them. In this way, the output torque of the motor will generate a force (f_m) directly on the driven link. The direction of this force will always be perpendicular to the side links, so that the bearings will not experience any loading from the motor forces. Conversely, any external forces or torques applied to the driven link will be supported by the side links and bearings, except those forces aligned with the instantaneous motion direction. The motor can then be sized appropriately by only considering the external forces acting on the driven link along the motion arc.

The virtual fifth link acts as an epicyclic gear carrier output, with the motor pinion serving as the planet gear input and the drive surface serving as a stationary sun gear. This arrangement allows a modest increase in the transmission ratio as compared to two equivalent fixed-axis gears. The transmission ratio, η, defines the relationship between the motor angle θ_m and joint angle θ:

$$\theta_m = (l_1/r_d)\theta = \eta\theta. \quad (1)$$

[1]A. Quaid is with Vivero One Research, LLC, Hollywood, FL USA. aquaid(at)vivero1.com

[2]It's not a typo! Arctuator™ is a trademark of Vivero One Research, LLC. U.S. Patent 8,464,603. Additional U.S. and Int'l. patents pending.

Although eight bearings are required per module, because they share the load and are positioned in the far corners of the module, they can be relatively small and inexpensive, yet still be effective at supporting cantilevered and off-center loads.

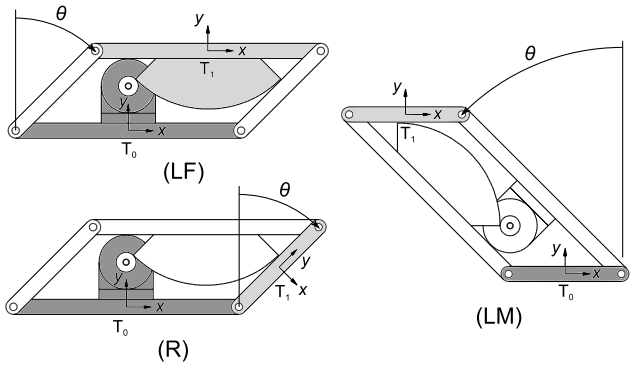

Fig. 2. An Arctuator module can be mounted in a large force (LF), large motion (LM), or rotation (R) configuration. All modules are shown with $\theta = +45°$, with the base link shown in dark gray and the output link shown in light gray.

As shown in Fig. 2, a module can be used in three different configurations. While each module can be modeled as a closed kinematic chain, when connecting multiple modules to form serial chain devices, it may be preferable to use a single homogeneous link transformation for each module.

In the *large force* (LF) configuration, the drive link is the base link and the driven link is the output link[1]. In this case, the output link will translate along an arc of radius l_1. Assuming the link coordinate frames are defined as shown in Fig. 2, the link transformation is given by:

$$ {}^0_1T_{LF} = \begin{bmatrix} 1 & 0 & 0 & l_1\sin(\theta) \\ 0 & 1 & 0 & l_1(1-\cos(\theta)) \\ 0 & 0 & 1 & 0 \\ 0 & 0 & 0 & 1 \end{bmatrix}. \quad (2) $$

In this configuration, the range of motion in the x direction will be $2l_1\sin(\theta_{max})$, where θ_{max} represents half of the angular range of motion of the module angle θ. There will also be a motion of $l_1(1-\cos(\theta_{max}))$ in the y direction, which will generally be undesirable. For this reason, multiple modules will normally be combined and controlled in a coordinated fashion to provide the desired planar or spatial motion capabilities, much like using multiple revolute joints to provide straight-line motion. However, as noted, the output of a multiple-module Arctuator device will maintain a constant orientation without requiring additional actuators.

The force output along the instantaneous direction of motion, f_{LF}, will be simply $f_{LF} = \tau_m/r_d$, where τ_m is the motor torque.[2] Interestingly, the force output is not dependent on the link lengths for this mounting configuration.

In the *large motion* (LM) configuration, one side link is the base link and the opposite side link is the output link. The output link will again translate along an arc, but with a larger radius of l_2. Assuming the link coordinate frames are defined as shown in Fig. 2, the link transformation is given by:

$$ {}^0_1T_{LM} = \begin{bmatrix} 1 & 0 & 0 & -l_2\sin(\theta) \\ 0 & 1 & 0 & l_2(1-\cos(\theta)) \\ 0 & 0 & 1 & 0 \\ 0 & 0 & 0 & 1 \end{bmatrix}. \quad (3) $$

In this configuration, the range of motion in the x direction will be $2l_2\sin(\theta_{max})$, with a motion of $l_2(1-\cos(\theta_{max}))$ in the y direction. The force output along the instantaneous direction of motion will be $f_{LM} = (l_1/l_2)(\tau_m/r_d)$. The force output is proportional to the ratio of the link lengths for this mounting configuration. Assuming that l_2 is double l_1, the force output for this configuration will be half that of the LF configuration, while the motion range will be double. The motor body will also move as θ changes, increasing the effective gravity load and moving inertia relative to the LF configuration.

In the *rotation* (R) configuration, any link can be used as the base link with an adjacent link as the output link. The output link will now rotate about the shared pivot joint. Assuming the link coordinate frames are defined as shown in Fig. 2, the link transformation is given by:

$$ {}^0_1T_{R} = \begin{bmatrix} \cos(\theta) & \sin(\theta) & 0 & l_2/2 + l_1\sin(\theta)/2 \\ -\sin(\theta) & \cos(\theta) & 0 & l_1(1-\cos(\theta))/2 \\ 0 & 0 & 1 & 0 \\ 0 & 0 & 0 & 1 \end{bmatrix}. \quad (4) $$

The output torque, τ_R, for this mounting configuration is given by $\tau_R = \eta\tau_m = (l_1/r_d)\tau_m$. In practice, Arctuator modules are limited to angular ranges of motion of approximately $\pm 45°$, limiting their applicability as general purpose rotational joints. However, having this mounting configuration available increases the versatility of the module, allowing them to be used for applications where modest rotation ranges are sufficient.

Of course, robots and other mechanical devices have long incorporated four-bar and five-bar linkages [3], [4], [5], [6]. However, in most cases, these linkages are tightly integrated into the rest of the arm design and therefore not suitable as modular actuators. There has also been much interest in modular robotic actuators, especially for self-reconfigurable devices [7], [8], [9], extremely low cost applications [10], or hyper-redundant devices [11].

III. Modularity

Arctuator modules have limited usefulness unless multiple modules are connected together. One possible modular connection scheme is shown in Fig. 3. Each link includes features for mechanical and electrical connections between modules. On the drive link and one of the side links, uniform pitch patterns of through holes are provided so that these links can be fastened to a base plate or proximal module. On the driven link and the remaining side link, patterns of

[1] Assuming that $l_1 < l_2$.

[2] This result is easy to confirm by examining a free-body diagram of the output link.

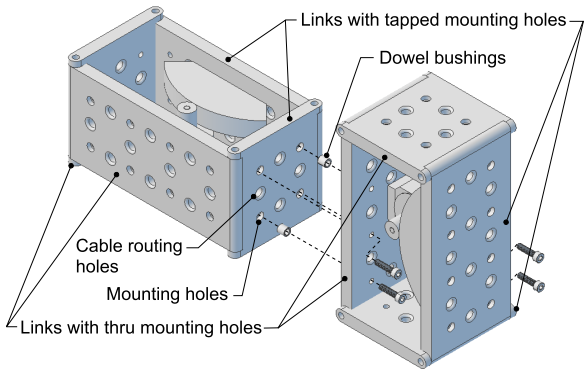

Fig. 3. Each Arctuator module has two links with tapped holes and two links with thru holes for inter-module mechanical connections. Holes for internal routing of electrical cables are also provided. The hole patterns provide 28 possible mounting possibilities between each pair of modules.

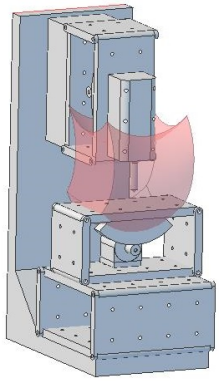

Fig. 4. Three modules with LF mounting combine to provide the 3D workspace shown.

matching threaded holes are provided so that end-effectors or distal modules can be attached. In addition, counter-bored holes coincident with both types of mounting holes allow for the use of optional hollow dowel bushings (e.g. Spirol DB100) for improved connection accuracy and integrity. Normally, each mechanical connection will utilize at least four screws and up to two dowel bushings. The mounting hole pattern allows for 28 unique mounting possibilities between adjacent modules.

Also shown in Fig. 3, a second pattern of through holes with rounded edges is provided on all four links for routing of inter-module electrical cables. Each module will have internal electronics including a microcontroller, bus transceiver, and power conditioning to allow for a simple four-wire connection between modules (two 24 VDC power and two bus signal lines). Vibration resistant spring-cage terminal blocks (e.g. Wago series 218) on the internal electronics eliminate the need to install connectors on the inter-module cables, simplifying cable routing and installation. For any of the 28 mechanical mounting configurations, at least four of the electrical routing holes will be aligned, allowing for separate routing of signal and power connections or internal routing of additional wires for end-effector tooling.

This electrical connection scheme allows the user to choose appropriate wire gauge, shielding, flexibility, and durability for a particular application. However, other module connection schemes are possible. The flat links of the modules have space to accommodate alternative mechanical and electrical coupling designs, including those that enable quicker and easier reconfiguration of modules. Also, a relatively large percentage of the volume within the parallelogram of each module is free space that could be used to mount additional on-board electronics and batteries, allowing for the possibility of wireless operation.

Despite their limited range of motion, Arctuator modules can be combined into a variety of useful devices. For example, three modules can be mounted in the large force configuration as shown in Fig. 4. The workspace of the device, shown as a translucent object, depicts the possible tip positions of the end-effector relative to lower modules, assuming $\theta_{max} = 45°$. The workspace will scale with the size of the modules, specifically their link lengths l_1. The bottom module is shown as a double width module, but a single width module could be substituted if overhang is acceptable. This configuration could be used for a variety of applications, including 3D printing, precision assembly, and perhaps light duty machining.

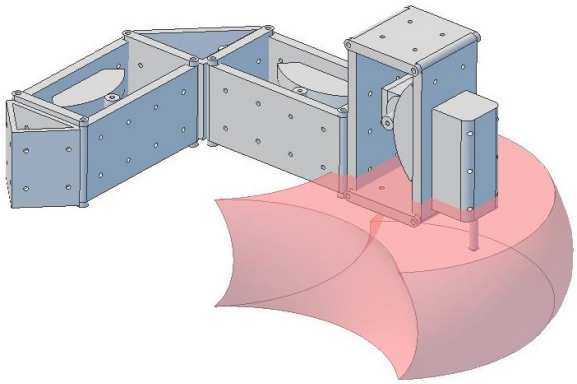

Fig. 5. Three modules combine to provide a SCARA like design.

Fig. 5 shows a SCARA-like configuration. As depicted, two of the three modules are mounted in a large motion mounting while one is mounted in a large force mounting. Fixed 90° gussets with suitable hole patterns serve as the connection to ground and to connect the first two modules. This configuration would be suitable for applications where the vertical motion range is relatively small and the vertical force requirements are relatively high compared to the horizontal directions. Although the workspace is small compared to what one would expect from a proportionally sized SCARA manipulator, this smaller workspace can be adjusted for a particular application by reconfiguring the modules appropriately.

Arctuator modules can also be combined with conventional actuators. Fig. 6 shows two modules combined with a conventional revolute base joint. As depicted, the two modules are mounted in a large motion mounting such that

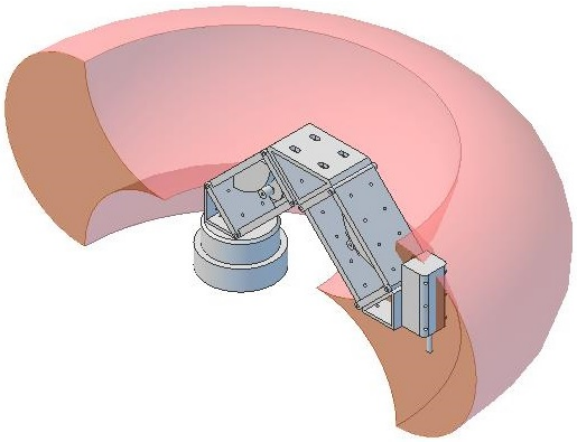

Fig. 6. Arctuator modules can be combined with conventional actuators. (The translucent workspace is shown cross-sectioned for improved visualization.)

they sweep out a toroidal volume as the revolute joint rotates, yielding a relatively large volume workspace. Similarly, one can imagine replacing the vertical module in Fig. 4 with a conventional translation joint for applications where precise linear motion is required (drilling, reaming, boring, etc.).

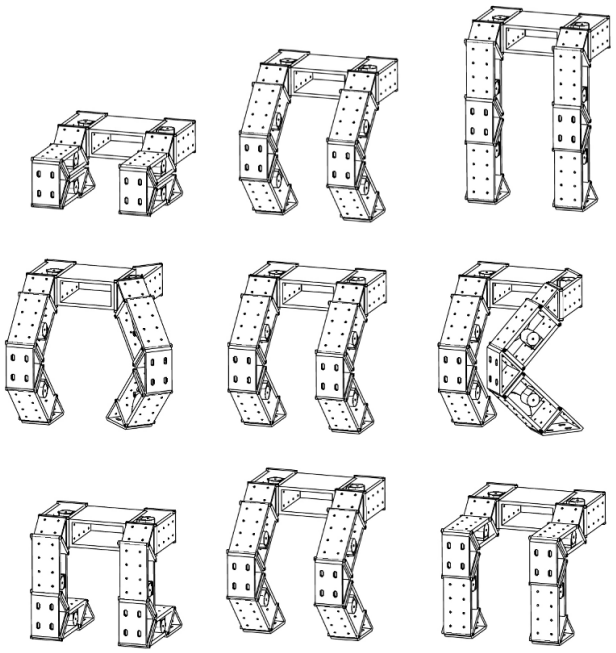

Fig. 7. Six Arctuator modules configured for use as a pair of 3-DOF legs.

Finally, Fig. 7 shows a pair of legs, each constructed from three modules. The top figures depict fully flexed to fully extended motion. The middle figures depict internal and external rotation of one leg. The bottom figures depict forward and backward motion, transitioning from a kneeling pose to a sitting pose. Note that the bottom of the feet will stay parallel to one another and the body of the device, making the legs better suited for relatively level terrain or for applications where it is important to minimize body roll.

IV. Preliminary results

A prototype Arctuator module, shown with two different loads in a large force mounting configuration in Fig. 8, has link lengths $l_1 = 90$ mm and $l_2 = 180$ mm and an angular motion range of $-45° \leq \theta \leq 45°$. It has a cable transmission driven by a hybrid stepping motor with an effective drive radius of $r_d = 5.5$ mm, yielding a transmission ratio of $\eta = 16.4$. A reflective encoder is used to provide sensing of the load side of the transmission.

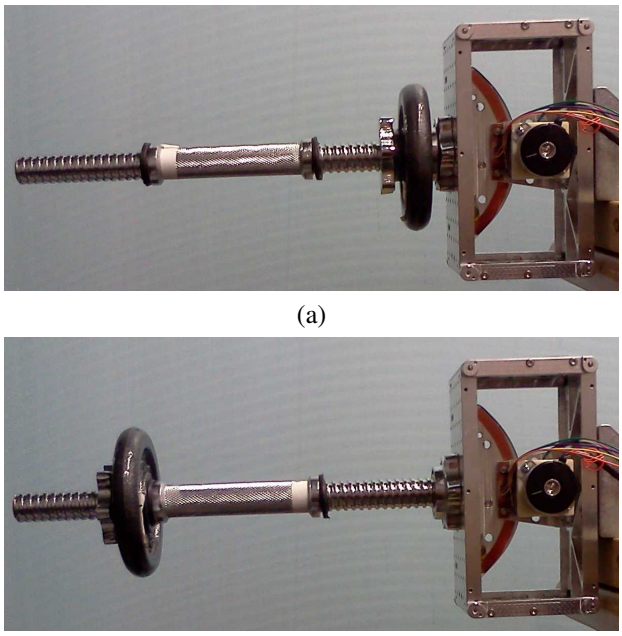

(a)

(b)

Fig. 8. Prototype module in LF mounting configuration. A 2.79 kg load has center of mass located (a) 93 mm or (b) 200 mm from the mounting surface of the output link.

The four links, drive surface, and motor mount are custom machined aluminum parts. The pivot joints connecting the links are standard 3.2 mm (1/8 in.) hardened dowel pins fixed to the long links and rotating in inexpensive ($2 ea.[3]) low-friction plastic (Rulon-J) bushings mounted in the short links. Precision dimensions on the machined parts are limited to the spacing between the joint pivots (important to ensure that the module is a parallelogram and opposite links remain parallel), and the width of the links (important so that the bushings are axially pre-loaded properly). A cable transmission is used rather than a geared transmission to minimize backlash and because it allows relatively relaxed tolerances on the drive surface and motor mount. In high-volume production, the links and other machined parts can be instead cast with a limited amount of finish machining, allowing for decreased production costs.

The motor is a NEMA 17 hybrid stepping motor (Lin Engineering WO-4118L-01D, $73) with 200 full steps per revolution and a nominal 0.59 Nm holding torque. For these

[3]All reference prices are in U.S. dollars for low quantity purchases as of July 2013.

experiments, the motor is driven by a motor driver IC (TI DRV8842) on a custom PCB with analog current commands for each phase provided by a microcontroller. In addition, a 20,000 count encoder (Encoder Products Co. Accu-coder FV00294) is mounted on the back shaft of the motor for testing purposes.

As noted in Sec. II, the transmission ratio and output force is inversely proportional to the effective drive radius r_d. Unfortunately, making the drive radius too small shortens the life of the cable. For example, one manufacturer recommends a pulley diameter of at least 15 times the cable diameter for stainless steel 7x49 construction cables[12]. Synthetic fibers, such as liquid crystal polymer (LCP) (Vectran), aramids (Kevlar, Twaron, Technora) or oriented-strand gel spun high-density polyethylene (HDPE) (Dyneema, Spectra) have high strength and very fine strands, allowing them to bend around small pulleys. They have been investigated for use in robotics [13], [14], [15], [16]. However, most HDPE fibers have significant creep, making them unsuitable for pre-tensioned cable drives. While the LCP and aramid fibers exhibit little to no creep, they have relatively poor wear resistance. Somewhat recently, new proprietary higher-strength and low creep HDPE materials (Dyneema SK-90 and SK-78) have become available.

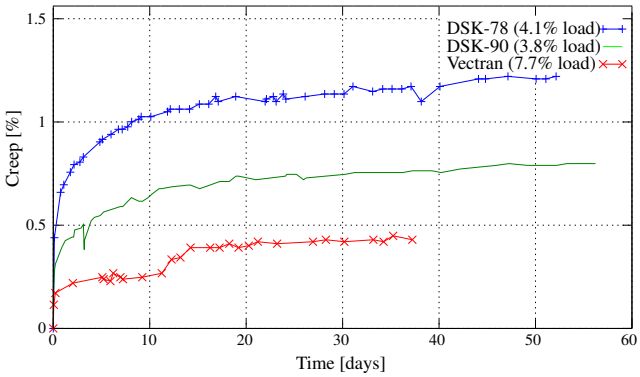

Fig. 9. Creep testing results for three synthetic fiber cables. Percentages noted indicate the load relative to the breaking strength of the cables.

A creep test was performed for several materials by terminating a section of cable with figure-eight stopper knots with steel electrical ring terminals. For each sample, a static load was applied and the distance between the ring terminals was measured with calipers over an extended period of time. A LCP fiber rope (Marlow Excel Vectran 2 mm diameter, 1570 N break strength, with the polyester cover removed), and two HDPE ropes (Marlow DSK-90 4G Kiteline, 1.4 mm diameter, 3110 N break strength, and Maffioli DSK-78 Ultra 2 mm diameter, 4500 N break strength) were tested. Results in Fig. 9 show an initial break-in period, likely partially due to the figure-eight knot tightening, followed by very little creep for all three samples.

A wear test was also performed on the DSK-90 cable. The cable was wrapped one turn around a smooth 10 mm motor pinion and preloaded to 88 N. The motor was repeatedly cycled by one revolution until cable failure. The DSK-90 sample broke at approximately 158k cycles, although significant wear was noticeable at 80k cycles. This lifetime is sufficient for many low-duty cycle applications. If higher duty cycles are required, a larger r_d (sacrificing output torque), a different cable material, or an appropriately grooved motor pinion[16] could be used. Alternatively, a geared drive could be substituted for the cable drive if increased backlash and/or friction is acceptable.

Based on these results, the DSK-90 cable (inexpensive at $\sim$\$1 per m) was chosen for the prototype module, terminated at each end to mounting points on the faces of the drive surface, with one end pre-tensioned with a spring to approximately 85 N. A 10 mm diameter smooth pinion is mounted on the motor shaft and the cable is wrapped four times around the motor pinion, relying on capstan friction [17] to prevent slippage and avoiding the need to provide cable termination features on the motor pulley.

Fig. 10. An encoder scale can be included on the output link to measure the load side of the transmission. A linear scale with 2.95 lines per mm for a reflective encoder is shown on the drive surface of the prototype module.

The face of the drive surface includes a custom reflective encoder scale with 2.95 lines per mm, as shown in Fig. 10. The scale is configured to detect the linear translational motion of the module along the principal motion direction. An inexpensive ($<$\$9) reflective encoder readhead (Avago AEDR-8300K) on a small prototype PCB attaches to the face of the motor, centered above the motor shaft. With quadrature output, the encoder provides a nominal 11.8 counts per mm resolution. This resolution yields approximately eight quadrature counts per stepper motor electrical cycle, which is sufficient resolution for detecting the hard stops during homing and for detecting transmission slippage and missed steps.

In the next iteration of the prototype, a second reflective encoder (Avago AEDR-8500, \$18) will be used to measure the motor shaft angle for improved fault detection and closed-loop control. It will be integrated into the same PCB as the load encoder. A small custom reflective code wheel will be mounted on the front shaft of the motor, facing back toward the front of the motor, with a diameter of $<$25 mm providing 3,300+ counts per revolution (cpr). This encoder is simulated in the experiments by discarding the lower three bits of the 20,000 cpr motor encoder, yielding 2,500 cpr. Nominal specifications for the Arctuator prototype are summarized in Table I.

The first experiment is intended to evaluate the dynamic

TABLE I

NOMINAL SPECIFICATIONS FOR ARCTUATOR PROTOTYPE.

Specification	Mounting configuration LF	LM	R
Size (for $\theta = 0°$)	102x192x97 mm		
Mass	1.33 kg		
Max. static load	107 N	53.6 N	9.65 Nm
Arcuate range of motion	141 mm	283 mm	90°
Linear range of motion in principal motion direction	127 mm	255 mm	n/a
Arcuate (or angular) motion resolution using 2500 cpr motor encoder	14 μm	28 μm	154 μrad
Linear (or angular) motion resolution using 11.8 counts/mm load encoder	85 μm	169 μm	<1.4 mrad

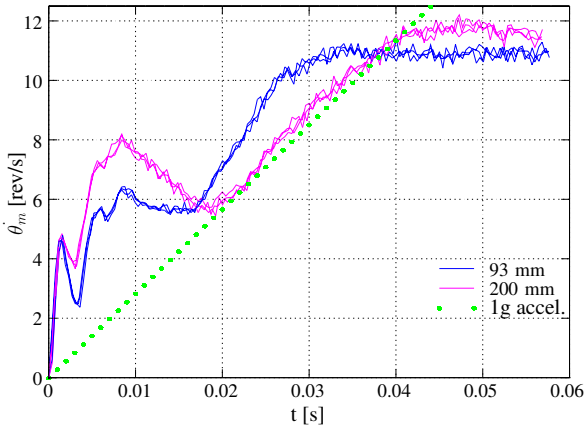

Fig. 11. Maximum-torque motor velocities for LF mounting and two cantilever load distances (Fig. 8). The dotted reference line is the velocity that would result from a constant 1g acceleration of the output link.

performance limits of the Arctuator prototype when mounted in the large force configuration for two cantilevered load configurations. Adjustable weights are mounted to the output link as shown in Fig. 8. The microcontroller runs a commutator at 25 kHz using the 2,500 cpr motor encoder as a motor position measurement. The commutator commands motor phase currents of $i_a = i_{max} \sin(n_p(\theta_m + \dot{\theta}_m T + \phi))$ and $i_b = i_{max} \cos(n_p(\theta_m + \dot{\theta}_m T + \phi))$, where $i_{max} = 2.8\ A$ is the maximum continuous current rating of the motor, $T = 40\mu$sec is a phase advance time, ϕ is a fixed phase offset such that the currents will produce the maximum torque in the positive direction, and $n_p = 50$ is the number of electrical cycles per motor revolution. The test is started at a motor position of $\theta_m = -\pi$ relative to the center of the workspace and the experiment is halted once the module reaches $\theta_m = 0$. This process is repeated several times for each loading configuration.

The first load, shown in Fig. 8(a), is a 2.79 kg mass with a center of mass 93 mm from the mounting surface of the output link. The second load is the same 2.79 kg mass reconfigured to have a center of mass 200 mm from the mounting surface. Figure 11 shows the motor velocity for three trials for each loading condition. The velocity is computed by differencing the full-resolution 20,000 cpr motor encoder. Note that the local slopes of the velocity curves represent instantaneous accelerations. The dotted reference line shows the motor velocity that would result in a 1 g acceleration of the load along the arc of motion.

For all experiments, the results show a substantial oscillation at the start of the motion and a roll-off in acceleration as the motor velocity exceeds 10 revolutions per second (rps). The roll-off is expected for the stepper motor at these velocities[18]. The oscillations are likely the result of the large load interacting with the compliances in the drive cable and the load mounting.

Despite these effects, the module appears capable of accelerating a load of 2.79 kg upward at an acceleration of 1g up to a maximum motor velocity of 10 rps for either loading condition. This motor velocity, which corresponds to a translational load velocity of 345 mm/s (along the output arc), seems sufficient for most purposes given that the total range of motion along the arc is 141 mm. Although the oscillations noticeably and repeatably change with the different loading conditions, both motions reach the end position at nearly identical times, suggesting that the 200 mm cantilevered load does not significantly increase dissipative friction in the bearings or elsewhere in the system compared to the 93 mm cantilevered load.

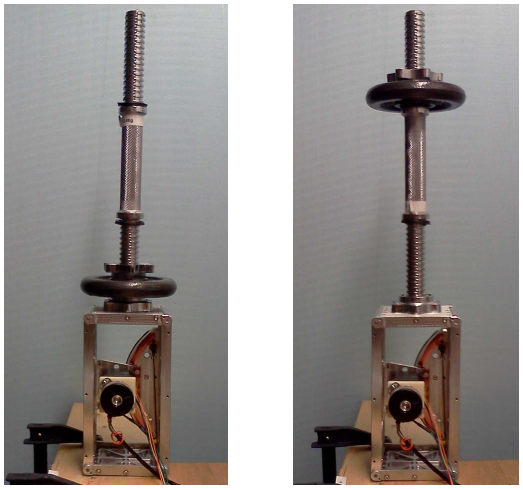

(a) (b)

Fig. 12. Prototype module in LM mounting configuration. A 2.79 kg load has center of mass located (a) 93 mm or (b) 200 mm from the mounting surface of the output link.

In the second experiment, the Arctuator prototype is mounted in the large motion configuration, as shown in Fig. 12. The experiment is otherwise the same as the first experiment. Figure 13 shows the motor velocity for three trials for each loading condition. The dotted reference line shows the motor velocity that would result in a 1 g acceleration of the output link along the arc of motion. This slope is different than in the first experiment because the output link moves twice as far per motor revolution for this mounting configuration. As before, there is a substantial oscillation at the start of the motion. Roll-off is less obvious as the end

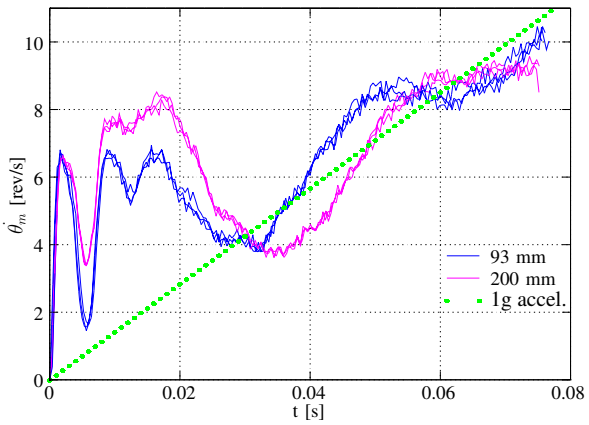

Fig. 13. Maximum-torque motor velocities for LM mounting and two cantilever load distances (Fig. 12). The dotted reference line is the velocity that would result from a constant 1g acceleration of the output link.

position is reached just as the velocity reaches 10 rps.

In this mounting configuration, the actuator appears capable of accelerating a load of 2.79 kg at nearly 1g up to a motor velocity of around 8 rps for either loading condition. This motor velocity, which corresponds to a translational output velocity of 553 mm/s (along the output arc), seems sufficient for most purposes given that the total range of motion along the arc is 283 mm. The oscillations noticeably and repeatably change with the different loading conditions, but both motions reach the end position at nearly identical times, suggesting as before, that the more cantilevered load does not significantly increase dissipative friction in the bearings or elsewhere in the system. Future work will investigate using feedback from both the load and motor encoders to reduce the load oscillations.

V. Conclusions

This work introduces a novel modular actuator technology. It attempts to demonstrate the usefulness of this technology by characterizing the dynamic performance of a prototype module and presenting concept designs that suggest the types of systems that can be constructed from combinations of these modules.

Many variations of Arctuator modules are possible, including larger or smaller modules, modules with different link aspect ratios, modules with geared transmissions, modules with composite links, and injection molded modules with living hinge pivot joints[19].

References

[1] B. Siciliano and O. Khatib, Eds., *Springer Handbook of Robotics*. Springer-Verlag, 2008, ch. 3.7 Joint Mechanisms.

[2] A. Slocum, *Precision Machine Design*. Soc. of Manufacturing Engineers, 1992.

[3] J. J. Craig, *Introduction to robotics: mechanics and control*. Addison-Wesley, 1989, ch. 3.

[4] J. Y. S. Luh and Y.-F. Zheng, "Computation of input generalized forces for robots with closed kinematic chain mechanisms," *Robotics and Automation, IEEE Journal of*, vol. 1, no. 2, pp. 95–103, 1985.

[5] H. Kazerooni and S. Kim, "A new architecture for direct drive robots," in *Robotics and Automation, 1988. Proceedings., 1988 IEEE International Conference on*, Apr., pp. 442–445 vol.1.

[6] T. H. Massie and J. J. Kenneth Salisbury, "Force reflecting haptic interface," U.S. Patent 5,587,937, Dec. 24, 1996.

[7] D. Rus and M. Vona, "A physical implementation of the self-reconfiguring crystalline robot," in *Robotics and Automation, 2000. Proceedings. ICRA '00. IEEE International Conference on*, vol. 2, pp. 1726–1733 vol.2.

[8] J. Suh, S. Homans, and M. Yim, "Telecubes: mechanical design of a module for self-reconfigurable robotics," in *Robotics and Automation, 2002. Proceedings. ICRA '02. IEEE International Conference on*, vol. 4, pp. 4095–4101 vol.4.

[9] S. Murata, E. Yoshida, A. Kamimura, H. Kurokawa, K. Tomita, and S. Kokaji, "M-tran: self-reconfigurable modular robotic system," *Mechatronics, IEEE/ASME Transactions on*, vol. 7, no. 4, pp. 431–441, Dec.

[10] M. Catalano, G. Grioli, M. Garabini, F. Bonomo, M. Mancinit, N. Tsagarakis, and A. Bicchi, "Vsa-cubebot: A modular variable stiffness platform for multiple degrees of freedom robots," in *Robotics and Automation (ICRA), 2011 IEEE International Conference on*, May, pp. 5090–5095.

[11] C. Wright, A. Buchan, B. Brown, J. Geist, M. Schwerin, D. Rollinson, M. Tesch, and H. Choset, "Design and architecture of the unified modular snake robot," in *Robotics and Automation (ICRA), 2012 IEEE International Conference on*, May, pp. 4347–4354.

[12] *Design guide for cable solutions*, Sava Industries, Inc., 2006, rev 6/10, DG1007.

[13] S. Jacobsen, E. Iversen, D. Knutti, R. Johnson, and K. Biggers, "Design of the Utah/M.I.T. dextrous hand," in *Robotics and Automation. Proceedings. 1986 IEEE International Conference on*, vol. 3, Apr., pp. 1520–1532.

[14] S. Ma, S. Hirose, and H. Yoshinada, "Design and experiments for a coupled tendon-driven manipulator," *Control Systems, IEEE*, vol. 13, no. 1, pp. 30–36, 1993.

[15] U. Seibold, B. Kubler, and G. Hirzinger, "Prototype of instrument for minimally invasive surgery with 6-axis force sensing capability," in *Robotics and Automation, 2005. ICRA 2005. Proceedings of the 2005 IEEE International Conference on*, April, pp. 496–501.

[16] M. P. Summers, "Rope selection for rope drive transmissions used in robotic manipulation," Oregon State University, Tech. Rep., 2010, honors Thesis BSME.

[17] J. Flory and J. Hagedorn, "Proper use of fiber ropes on capstans and bitts," in *OCEANS 2003. Proceedings*, vol. 2, 2003, pp. 1064–1069.

[18] *2011-2012 Catalog*, Lin Engineering.

[19] A. E. Quaid, "Parallelogram based actuating device," U.S. Patent 8,464,603, June 18, 2013.